SPECT imaging of Lysyl Oxidase-Like 2 in a model of idiopathic pulmonary fibrosis

Romane Vizier, Anaïs-Rachel Garnier, Alexandre Dias, Mathieu Moreau, Michael Claron, Bertrand Collin, Franck Denat, Pierre-Simon Bellaye, Victor Goncalves

SPECT imaging of Lysyl Oxidase-Like 2 in a model of idiopathic pulmonary fibrosis

Romane Vizier,[1] Anaïs-Rachel Garnier,[2] Alexandre Dias,[2] Mathieu Moreau,[1] Michael Claron,[1] Bertrand Collin,[1,2] Franck Denat,[1] Pierre-Simon Bellaye,[2,¥,*] Victor Goncalves[1, ¥,*]

[*] Corresponding authors: Victor Goncalves: victor.goncalves@u-bourgogne.fr; Pierre-Simon Bellaye: psbellaye@cgfl.fr

[¥] These authors contributed equally to this work

[1] Institut de Chimie Moléculaire de l'Université de Bourgogne, UMR 6302, CNRS, Université de Bourgogne, 9 avenue Alain Savary, 21078 Dijon Cedex, France.

[2] Centre Georges François Leclerc, Service de Médecine Nucléaire, Plateforme d'Imagerie et de Radiothérapie Précliniques, 1 rue du Professeur Marion, 21079 Dijon Cedex, France.

ORCID:

Romane Vizier: 0000-0001-6548-4040

Anaïs-Rachel Garnier:

Alexandre Dias:

Mathieu Moreau: 0000-0003-1429-8461

Michael Claron: 0000-0001-8949-7452

Bertrand Collin: 0000-0002-0360-0664

Franck Denat: 0000-0002-9652-4006

Pierre-Simon Bellaye: 0000-0002-8498-5163

Victor Goncalves: 0000-0001-9854-4409

Abstract

Non-invasive imaging of idiopathic pulmonary fibrosis (IPF) remains a challenge. The aim of this study was to develop an antibody-based radiotracer targeting Lysyl Oxidase-like 2 (LOXL2), an enzyme involved in the fibrogenesis process, for SPECT/CT imaging of pulmonary fibrosis.

The bifunctional chelator DOTAGA-PEG_4-NH_2 was chemoenzymatically conjugated to the murine antibody AB0023 using microbial transglutaminase, resulting in a degree of labeling (number of chelators per antibody) of 2.3. Bio-layer interferometry (BLI) confirmed that the binding affinity of DOTAGA-AB0023 to LOXL2 was preserved with a dissociation constant of 2.45 ± 0.04 nM. DOTAGA-AB0023 was then labeled with ^{111}In and *in vivo* experiments were carried out in a mice model of progressive pulmonary fibrosis induced by intratracheal administration of bleomycin. [^{111}In]In-DOTAGA-AB0023 was injected in three groups of mice (control, fibrotic and treated with nintedanib). SPECT/CT images were recorded over 4 days p.i. and an *ex vivo* biodistribution study was performed by gamma counting. A significant accumulation of the tracer in the lungs of the fibrotic mice at D18 post-bleomycin. Interestingly, the tracer uptake was found selectively upregulated in fibrotic lesions observed on CT scans. Images of mice that received the antifibrotic drug nintedanib from D8 up to D18 showed a decrease in [^{111}In]In-DOTAGA-AB0023 lung uptake associated with a decrease in pulmonary fibrosis measured by CT scan.

In conclusion, we report the first radioimmunotracer targeting the protein LOXL2 for nuclear imaging of IPF. The tracer showed promising results in a preclinical model of bleomycin-induced pulmonary fibrosis, with high lung uptake in fibrotic areas and accounted for the antifibrotic activity of nintedanib.

Keywords

Idiopathic Pulmonary Fibrosis, Lysyl Oxidase-Like 2, SPECT/CT, DOTAGA, Site-specific conjugation

Table of Contents Graphic

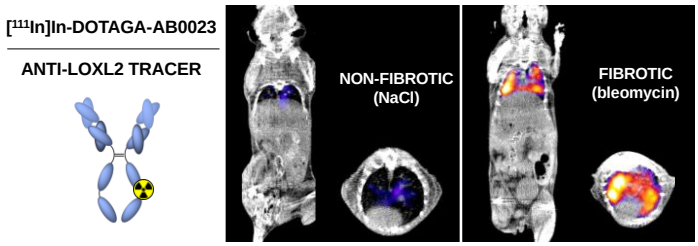

Introduction

Idiopathic pulmonary fibrosis (IPF) is a chronic and irreversible lung disease characterized by an alteration of the pulmonary architecture, caused by the excessive and progressive deposition of extracellular matrix (ECM) in the lung parenchyma [1]. This aberrant accumulation of ECM leads to the destruction of the lung structure and ultimately to a decline in lung function. Although this disease is rare, with an estimated incidence of 0.09 to 1.30 per 10,000 patients worldwide, its prevalence is increasing, and its prognosis is poor, with a median patient survival time of five years after diagnosis [2]. Therapeutic options remain limited to pirfenidone and nintedanib which only delay the progression of the disease without stopping it [3].

Despite significant progress, IPF diagnosis is still difficult. While a standard high-resolution computed tomography (HRCT) can confirm the diagnosis of IPF in cases where an interstitial pneumonia (UIP) pattern is present, the majority of patients may need a lung biopsy, which carries a high risk of morbidity and mortality [4]. Additionally, one of the primary imaging criteria for UIP, honeycombing, indicates an advanced stage of the illness. However, early diagnosis is important in IPF because delayed diagnosis is linked to worse outcomes and higher mortality [5]. In order to support early diagnosis, which could significantly reduce existing treatment delays, imaging biomarkers for early/active fibrosis are required.

Major clinical problems also include the absence of instruments to track the progression of the disease and the effectiveness of anti-fibrotic therapy. IPF progression is unpredictable; whereas some patients decline quickly and pass away within months, others experience a gradual decline and limited progression. Additionally, considering how differently IPF patients respond to pirfenidone and nintedanib from one another, those who do not respond to one drug may benefit from the other. The early prediction of treatment success is a crucial therapeutic concern given the potentially crippling adverse effects linked to these treatments. The first step towards a tailored management of IPF patients would therefore be to develop novel imaging predictive biomarkers to predict/monitor fibrosis progression and treatment success.

Lysyl Oxidase-like 2 (LOXL2), a copper-dependent amine oxidase, plays a key role in a wide range of fibrotic disorders, including pulmonary fibrosis. LOXL2 catalyzes the post-translational oxidative deamination of the ε-amino group of lysine in collagen and other proteins of the extracellular matrix into an aldehyde group (allysine). This aldehyde can react with other lysine or allysine residues in nearby proteins, allowing cross-linking of collagen to take place [6,7]. A number of studies have shown that the expression of LOXL2 in pulmonary fibroblasts increases drastically in case of fibrosis promoting the development of the disease [8–12]. Preclinical studies, conducted with a murine monoclonal antibody, AB0023, have shown that LOXL2 blockade inhibits partially LOXL2 activity, leading to a decrease in ECM production and reduced bleomycin-induced pulmonary fibrosis *in vivo* [11]. In addition, LOXL2 was found increased in fibrotic tissues and in sera from patients with IPF in association with increased risk for disease progression [7]. Further, an upregulation of LOXL2 has been shown in active area, fibroblastic foci, of diseased IPF lung tissue, with relatively low expression in healthy lung tissue. As a consequence LOXL2 is considered a major driver of fibrosis [11,13]. Therefore, simtuzumab, a humanized monoclonal antibody targeting LOXL2, was evaluated in phase 2 clinical trials [11,14–17]. Unfortunately, simtuzumab failed at clinical stage, with no significant therapeutic efficacy observed on patients [18–21]. These results are yet not fully explained, but may be related to insufficient inhibitory potency of the antibody or an inadequate selection of patients included in the trials.

The protein LOXL2 has not yet been explored as an imaging target. Wuest et al. reported in 2015 a [^{18}F]F-labeled tracer targeting Lysyl Oxidase (LOX), developed from an oligopeptide substrate of this enzyme (with a *K*m in the sub-millimolar range) [22]. However, this tracer is a pan-LOX substrate, and has shown rapid washout from LOX-expressing tissues and some degree of non-specific binding. A LOXL2-specific radiotracer could provide valuable information to facilitate in the staging of IPF patients, monitoring disease progression and response to treatments. In addition, it could improve the selection of patients most likely to respond to new LOXL2 inhibitors currently in development [23–26]. Herein, we report the development and preclinical evaluation of a radiotracer targeting LOXL2, based on the murine antibody AB0023. The antibody was conjugated to the metal chelator DOTAGA, radiolabeled with ^{111}In and evaluated in a mice model of pulmonary fibrosis, induced by intratracheal administration of bleomycin, by SPECT/CT and biodistribution studies [27].

Materials and methods

Reagents and equipment specifications

AB0023 was produced by Proteogenix (France) and Biointron (China). DOTAGA-PEG$_4$-NH$_2$ was kindly given by Chematech (France). PNGase F was supplied by Promega (USA) in 20 mM Tris-HCl (pH 7.5), 50 mM NaCl and 5 mM EDTA at a concentration of 10 000 U/mL. mTGase was provided by Zedira (Germany) in PBS (Phosphate Buffer Saline) 0.1 M, pH 7.4, at a concentration of 280.8 U/mL. Recombinant human LOXL2 (fused with a polyhistidine tag at the C-terminus) was purchased from Sino Biological (China) and was reconstituted in ultrapure water.

HPLC analyses were conducted on a Thermo Scientific MAbPac column (4 µm, 50 x 2.1 mm) with the following eluents: A: H_2O + 0.08% FA + 0.02% TFA and B: MeCN + 0.08% FA + 0.02% TFA and a gradient program: 20% of B for 0.5 min, 20% to 55% of B in 5.5 min, 55% to 80% in 0.5 min, 80% of B for 1 min, 80% to 20% in 0.1 min, 20% of B for 2.5 min, at a flow rate of 0.5 mL/min at 80 °C. High-resolution mass spectrometry analyses were recorded on a Orbitrap Exploris 240 mass spectrometer (Thermo Scientific) equipped with an electrospray ionization source (H-ESI II). Spectra were deconvoluted on BioPharma Finder software (Thermo Scientific). Ultrapure water produced by a PURELAB Ultra system from ELGA was used throughout (18.2 MΩ.cm). UV spectroscopy was done on Mettler Toledo UV/Vis excellence UV5Nano.

Size-exclusion chromatography (SEC-HPLC) analyses were performed on a JASCO HPLC system LC-2000 analytical series equipped with a Superdex 200 5/150 GL column. Instant thin-layer chromatography (iTLC or radio-TLC) was performed using sheets impregnated with silica gel (iTLC-SG; Agilent), eluted with 0.1 M citrate buffer pH 6.0, and analyzed on an AR-2000 radio-TLC plate reader (Bioscan Inc.).

Synthesis of the bioconjugate

AB0023 was first deglycosylated using PNGase F. 2 µL of PNGase F (20 U) was added to 500 µg of AB0023 (3.4 nmol, in solution at 3.5 g/L in PBS pH 7.4). The mixture was incubated 8 h at 37°C in a Thermomixer (700 rpm). PNGase F was removed from the mixture by ultrafiltration on an Amicon Ultracel-50 kDa (Merck-Millipore) and the purified solution was centrifuged (4000 rpm, 20 min, 4 °C) to concentrate the product at 9.0

g/L. To perform the bioconjugation, DOTAGA-PEG_4-NH_2 (89 equivalents, 246 nmol, 4.1 µL of a 60 mM stock solution in PBS pH 7.4) was added to 400 µg of deglycosylated AB0023 (1 equivalent, 2.76 nmol, in solution at 9.0 g/L in PBS pH 7.4) followed by 4.7 µL (1.32 U) of mTGase (280.8 U/mL). The reaction mixture was incubated 6 h at 37 °C on a Thermomixer (700 rpm) and monitored by mass spectrometry. The bioconjugate was purified by SEC-FPLC on an Äkta Pure 25 M chromatography system (GE Healthcare Life Sciences) equipped with a Superdex 200 10/300 GL column, using $AcONH_4$ 0.1 M pH 5.4 as eluant. This eluant allowed the bioconjugate to be isolated directly in the radiolabeling buffer without further buffer exchange. The protein yield was calculated by measuring the absorbance at 280 nm by UV spectroscopy (ε_{280} = 1.4 $mL.mg^{-1}.cm^{-1}$).

BLI measurements

The affinity of AB0023 for rhLOXL2 was studied by biolayer interferometry (BLI) on a Sartorius Octet® R2 system. All experiments were performed at 30 °C with 1000 rpm shaking. Ni-NTA Dip and Read™ (Sartorius) biosensors were employed. LOXL2 was diluted in PBS to obtain a final concentration of 5 µg/mL. LOXL2 and AB0023 were used as the ligand and the analyte respectively in the experiments. PBS was used as control. Biosensors were first dipped into wells containing PBS during 10 min. The loading time of LOXL2 on the biosensors was 600 s. Two washes of the biosensors with PBS during 60 s were performed before the association step. Association time of AB0023 to LOXL2 was set at 600 s. Dissociation time was set at 900 s in PBS.

Raw sensorgrams were fitted using a 1:2 bivalent analyte model in Octet™ data analysis HT software v 12.2. Data were corrected with an alignment of the Y axis to the average of baseline step, an alignment of the inter-step to the association step and a Savitzky-Golay fittering.

Radiochemistry

476 µL of a [^{111}In]$InCl_3$ solution at 840 MBq/mL (400 MBq) was added to 708 µg of bioconjugate (1.9 mg/mL in $AcONH_4$ 0.1M pH 5.4). 47.6 µL of $AcONH_4$ 1 M was further added to neutralize the acidity of the [^{111}In]$InCl_3$ solution. The mixture was incubated 1 h at 37 °C in a Thermomixer (700 rpm). The reaction was monitored by radio-TLC. Unincorporated ^{111}In was scavenged by adding 47 µL of a solution of 50 mM EDTA in 0.1 M $AcONH_4$ pH 5.4. No further purification was needed. The final radiolabeling purity was measured by radio-TLC.

Animal experiments

All animal studies were conducted in accordance with the legislation on the use of laboratory animals (directive 2010/63/EU) and were approved by accredited Ethical committee (C2ea Grand Campus n°105) and the French Ministries of Research and Agriculture (project #12816).

Eight-week-old C57/Bl6 mice received at D0 a single intratracheal injection of 2 mg/kg of bleomycin (BLM, Santa Cruz biotechnology, USA) or NaCl (Control) under anesthesia (3% isoflurane). BLM-induced lung fibrosis is characterized by an initial inflammatory phase lasting from D0 to D7 which moves on to a progressive fibrotic phase from D7 to D23. BLM instillation was performed by a unique expert operator. Animal weights were monitored daily from D0 to D7 in order to select mice that responded to BLM (selection of animals with at least 10% weight loss from D0 to D7). For each experiment, approximately 20% of animals were excluded. When indicated, animals were treated with nintedanib (Ofev™, 60mg/kg) by daily gavage during the fibrotic phase of BLM-induced lung fibrosis from D7 to D18 as recommended [28].

In vivo imaging

One pilot study was performed on NaCl- and BLM-receiving mice at D18 post-BLM by SPECT/CT imaging with [^{111}In]In-DOTAGA-AB0023 (NaCl n=6, BLM D18 n=6). Mice were anesthetized through isoflurane (1.5%) inhalation for intravenous injection (tail vein) of [^{111}In]In-DOTAGA-AB0023 (10 MBq, 25 µg/mouse). Mice were then maintained under anesthesia (1.5% isoflurane) and placed on an imaging heated bed inside a NanoSPECT^{TM}-CT (Mediso, Hungary). A CT scan of a lung-centered region was obtained (500 ms, 45 kV, 180 projections, pitch 1, binning 1:4) followed by SPECT acquisition with 90−120 s per projection frame resulting in acquisition times of 45−60 min of the same region or a PET acquisition (30 minutes) of the same region (lung-centered, 250-700 keV). Images were taken 24 h, 48 h, 72 h and 96 h post-injection (p.i.) of [^{111}In]In-DOTAGA-AB0023.

In another experiment, imaging of lung fibrosis was performed on NaCl- (n=6) and BLM-receiving mice treated with vehicle (n=6) or nintedanib (n=5) by SPECT/CT with [^{111}In]In-DOTAGA-AB0023 at D18 following the same imaging protocol as described above.

For each experiment, after the last imaging (96 h p.i.), mice were sacrificed and major organs (blood, bladder, kidneys, spleen, liver, heart, muscle and lungs) were harvested for *ex vivo* quantification using a γ-counter (Wizard, Perkin Elmer).

Image analysis

All SPECT/CT fusion images were obtained using the VivoQuant^{TM} software (Invicro, USA). Each image was visually interpreted and 3D regions of interest (3DROI) corresponding to the lungs were manually drawn for CT quantification and to determine their radioactivity content. Injected doses per animal were measured at the time of injection in MBq. Lung radioactivity content was expressed in MBq, converted to percentage of injected dose per gram of tissue (% ID/g). All images were decay corrected for quantification. In addition, a semi-automatic segmentation of 3DROI was performed on CT scans as follows: normal lung density (-800 to -100 HU) corresponding to aerated lung areas and high lung density (-100 to 300 HU) corresponding to non-aerated/fibrotic lung areas as previously described [29]. This semi-automatic segmentation allowed the independent quantification of the radioactivity content of [^{111}In]In-DOTAGA-AB0023 in normal (aerated) and high (non-aerated) density lung tissue respectively.

Results

Conjugation of DOTAGA to AB0023

The recombinant murine antibody was deglycosylated using PNGase F and then conjugated to DOTAGA-PEG$_4$-NH$_2$ using microbial transglutaminase (Fig. 1). DOTAGA-AB0023 was obtained with 40% protein recovery yield over two steps. Native AB0023, deglycosylated AB0023 and the final bioconjugate and were analyzed by RP-HPLC-MS (Fig. 2A, 2B and 2C). After deglycosylation, the deconvoluted spectrum revealed a major peak at 144,974 Da corresponding to deglycosylated AB0023 (Fig. 2B). Two minor peaks (145,103 Da and 145,232 Da) were detected, corresponding to different degrees of C-terminal lysine clipping [30]. After conjugation, the deconvoluted spectrum showed a major peak at 146,329 Da corresponding to the covalent grafting of two

DOTAGA-PEG$_4$-NH$_2$ and a degree of labeling (DOL) of 2 (Fig. 2C). The additional peaks at 145,651 Da and 147,009 Da corresponded to DOL 1 and 3 respectively. LC-MS/MS analysis of DOTAGA-AB0023 after tryptic digestion enabled us to identify heavy chain residues Q153 and Q300 as those conjugated to DOTAGA-PEG$_4$-NH$_2$. The average DOL after 6 h of incubation at 37 °C was 2.3.

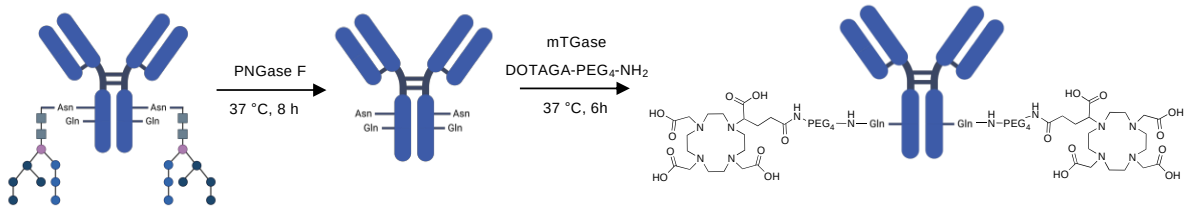

Fig. 1: Synthesis of the bioconjugate 1) PNGase F (20 U), PBS pH 7.4, 37 °C, 8 h; 2) DOTAGA-PEG$_4$-NH$_2$ (89 eq), mTGase (1.32 U), PBS pH 7.4, 37 °C, 6 h

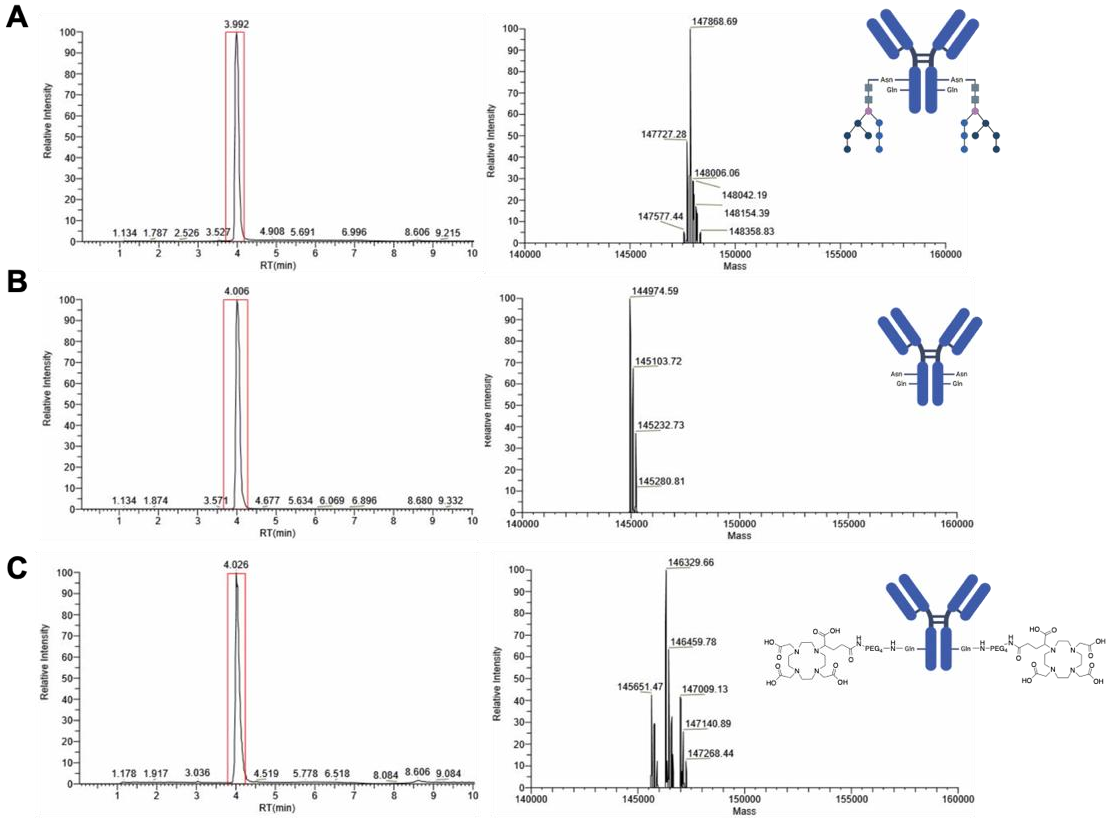

Fig. 2: Chromatograms and deconvoluted spectra of (A) native AB0023 (B) deglycosylated AB0023 and (C) DOTAGA-AB0023

Biolayer interferometry

Results of the BLI measurements demonstrated high affinity binding between native AB0023 and rhLOXL2 with a K_D of 0.89 ± 0.02 nM. Deglycosylated AB0023 and DOTAGA-AB0023 showed K_D equal to 2.43 ± 0.08 nM and 2.45 ± 0.04 nM respectively (Fig. 3). R^2 values for each measurement were >0.99.

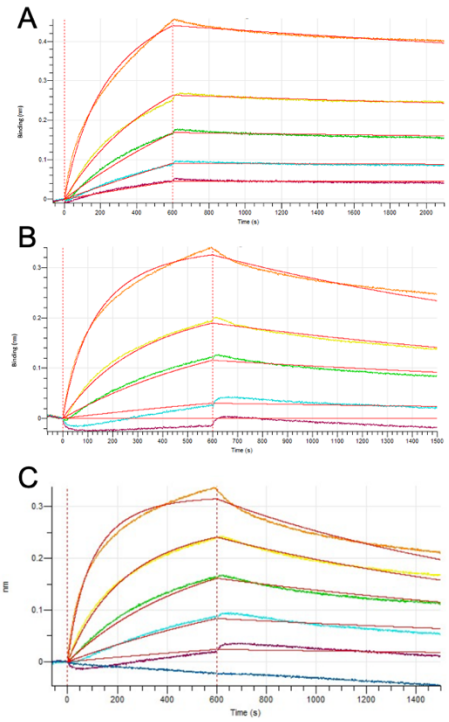

Color	Conc. (nM)
	20
	6.67
	2.22
	0.7407
	0.2469

Compound	Kd (nM)
AB0023	0.89 ± 0.02
Deglycosylated AB0023	2.43 ± 0.08
DOTAGA-AB0023	2.45 ± 0.04

Fig. 3: Kinetic analysis of (A) native AB0023 (B) deglycosylated AB0023 and (C) DOTAGA-AB0023

Radiolabeling

Radiolabeling yield of [^{111}In]In-DOTAGA-AB0023 reached 96% after 1 h at 37 °C with a specific activity equal to 570 MBq/mg (85 MBq/nmol) (supplemental fig. 3 A). This tracer proved to be stable *in vitro* over 7 days, in human plasma at 37°C (supplemental fig. 3 B).

***In vivo* imaging of LOXL2 can detect BLM-induced lung fibrosis**

NaCl and BLM-receiving mice underwent SPECT/CT imaging with the LOXL2 targeting agent [^{111}In]In-DOTAGA-AB0023 at D18 (Fig. 4A). SPECT/CT images were performed 24 h, 48 h, 72 h and 96 h post-injection of [^{111}In]In-DOTAGA-AB0023 showing that the best imaging time to differentiate NaCl- from BLM-receiving mice was 96 h post-injection (Fig. 4AB). The lung uptake of [^{111}In]In-DOTAGA-AB0023 was significantly increased in BLM-treated mice at D18 compared to non-fibrotic controls at 48 h, 72 h and 96 h (Fig. 4B). *Ex vivo* radioactivity quantification of the lungs confirmed the increase in [^{111}In]In-DOTAGA-AB0023 lung uptake 96 h p.i. in BLM-treated animals (Fig. 4C). In addition, lung to blood ratio and lung to muscle ratio demonstrated a clear increase in BLM-receiving mice compared with controls (Fig. 4DE). Similarly, lung CT of BLM-receiving mice showed an increase in fibrotic consolidations compared with control mice with an increase in mean lung density (MLD) and a decrease of aerated areas in BLM-treated mice compared with controls at D18 (Fig. 4FG). The global biodistribution of [^{111}In]In-DOTAGA-AB0023 demonstrated that uptake was not different between NaCl- and BLM-receiving mice except in the lungs (Fig. 4H). Time curves of lung/blood and lung/muscle ratio confirms that [^{111}In]In-DOTAGA-AB0023 is significantly increased in fibrotic lungs with an optimal signal-to-background ration at 96 h post-injection (Supplemental fig. 6A, B). Interestingly, discrimination of aerated and non-aerated lung areas by semi-automatic segmentation on CT scans demonstrated that [^{111}In]In-DOTAGA-AB0023 SPECT signal was only significantly increased in non-

aerated lung areas in BLM-receiving mice compared with control mice, showing the specificity of [^{111}In]In-DOTAGA-AB0023 for fibrotic areas (Fig. 4I). Interestingly, [^{111}In]In-DOTAGA-AB0023 lung uptake at 96 h significantly correlated with MLD measured on CT (Fig. 4J).

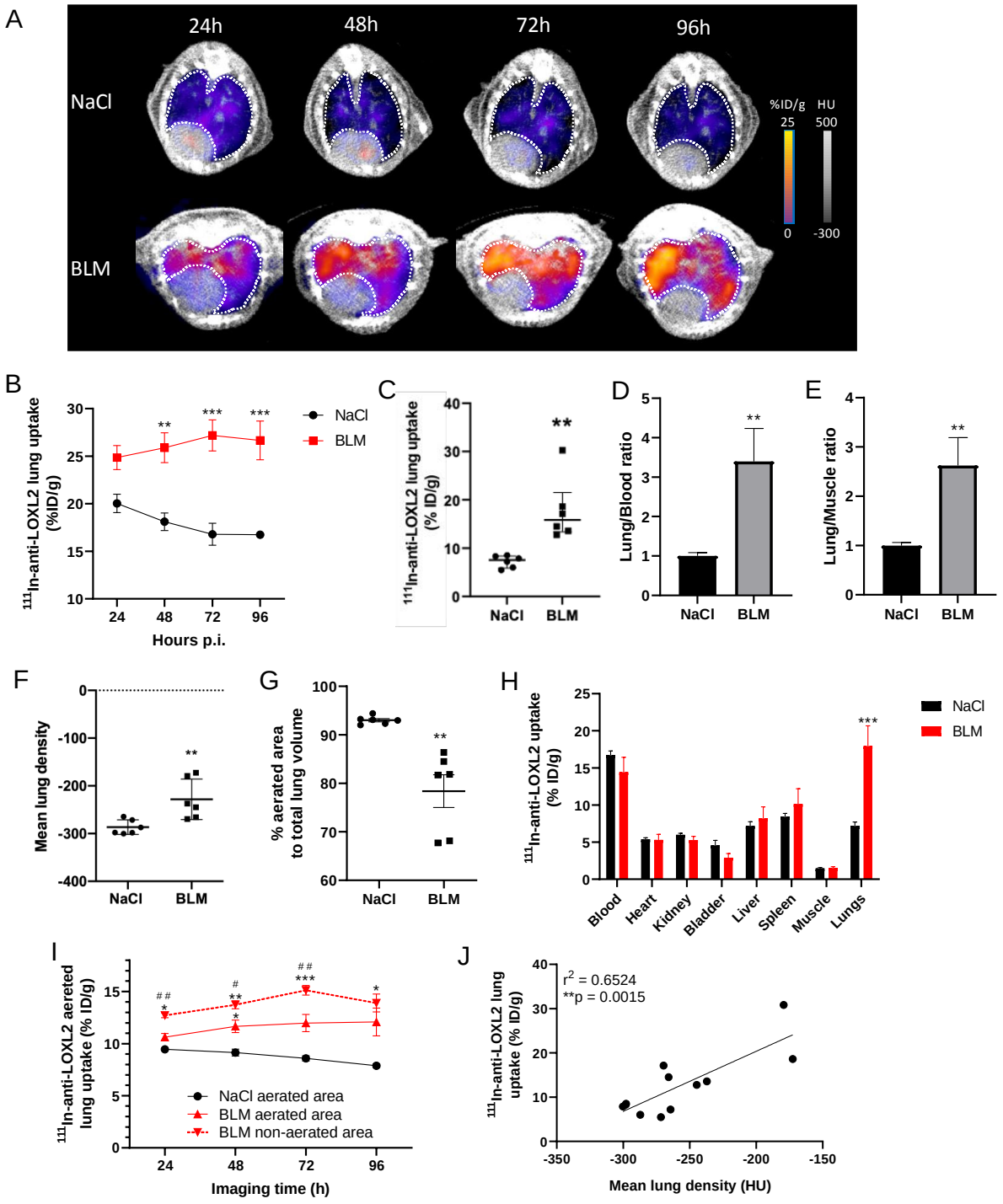

*Fig. 4: [^{111}In]In-DOTAGA-AB0023 is able to detect advanced BLM-induced lung fibrosis. A/ Representative lung SPECT/CT images with [^{111}In]In-DOTAGA-AB0023 of NaCl- and BLM-receiving mice at D18 at 24h, 48h, 72h and 96h p.i.. B/ Graph represents the [^{111}In]In-DOTAGA-AB0023 lung uptake in %ID/g measured on SPECT images of NaCl- and BLM-receiving mice at D18. Results are presented as mean ± SEM, NaCl n=6, BLM n=6. Difference between groups were compared using Mann-Whithney non-parametric t-test, **p<0.01, ***p<0.001. C/ Graph represents the [^{111}In]In-DOTAGA-AB0023 lung uptake in %ID/g measured by gamma-counting 96h p.i. of NaCl- and BLM-receiving mice at D18.*

*Results are presented as mean ± SEM, NaCl n=6, BLM n=6. Difference between groups were compared using Mann-Whithney non-parametric t-test, **p<0.01. D/ Graph represents the lung/blood ratio of [^{111}In]In-DOTAGA-AB0023 uptake in %ID/g measured by gamma-counting 96h p.i. of NaCl- and BLM-receiving mice at D18. Results are presented as mean ± SEM, NaCl n=6, BLM n=6. Ratios are normalized to 1 for the NaCl group. Difference between groups were compared using Mann-Whithney non-parametric t-test, **p<0.01. E/ Graph represents the lung/muscle ratio of [^{111}In]In-DOTAGA-AB0023 uptake in %ID/g measured by gamma-counting 96h p.i. of NaCl- and BLM-receiving mice at D18. Results are presented as mean ± SEM, NaCl n=6, BLM n=6. Ratios are normalized to 1 for the NaCl group. Difference between groups were compared using Mann-Whithney non-parametric t-test, **p<0.01. F/ Graph represents the mean lung density quantified on CT images of NaCl- and BLM-receiving mice at D18. Results are presented as mean ± SEM, NaCl n=6, BLM n=6. Difference between groups were compared using Mann-Whithney non-parametric t-test, **p<0.01. G/ Graph represents the percentage of aerated lung tissue measured on CT images of NaCl- and BLM-receiving mice at D18. Results are presented as mean ± SEM, NaCl n=6, BLM n=6. Difference between groups were compared using Mann-Whithney non-parametric t-test, **p<0.01. H/ Graph represents the [^{111}In]In-DOTAGA-AB0023 uptake in %ID/g measured by gamma counting in blood, heart, kidney, bladder, liver, spleen,muscle and lungs of NaCl- and BLM-receiving mice at D18. Difference between groups were compared using Mann-Whithney non-parametric t-test, ***p<0.001. I/ Graph represents the [^{111}In]In-DOTAGA-AB0023 lung uptake in %ID/g of NaCl- and BLM-receiving mice at D18 in aerated and non-aerated lung areas (segmented on CT images). Results are presented as mean ± SEM, NaCl n=6, BLM n=6. Stars (*) are representative of comparison of each group with NaCl group and hashs (#) are representative of statistical comparison of BLM aerated group with BLM non-aerated group. Difference between groups were compared using Mann-Whithney non-parametric t-test, *p<0.05, **p<0.01 and ***p<0.001. J/ Correlation between mean lung densities (HU) measured on CT images and [^{111}In]In-DOTAGA-AB0023 lung uptake (%ID/g) of corresponding lungs measured on SPECT/CT.*

In vivo imaging of LOXL2 is a useful tool to monitor the anti-fibrotic efficacy of nintedanib

NaCl and BLM-receiving mice treated or not with nintedanib underwent SPECT/CT imaging with [^{111}In]In-DOTAGA-AB0023 at D18 (Fig. 5A). We confirmed that the lung uptake of [^{111}In]In-DOTAGA-AB0023 was increased in BLM-receiving mice compared to control at D18 (Fig. 5AB). Interestingly, in BLM-receiving mice nintedanib treatment dramatically decreased [^{111}In]In-DOTAGA-AB0023 lung uptake at D18 (Fig. 5AB). These results were confirmed by gamma counting at 96 h p.i. in which [^{111}In]In-DOTAGA-AB0023 lung uptake was significantly higher in BLM-receiving mice and was decreased by nintedanib (Fig. 5C). In addition, lung to blood ratio demonstrated a clear increase in BLM-receiving mice compared with BLM mice treated with nintedanib and controls (Fig. 5D). Similarly, MLD measured on CT significantly increased in BLM-receiving mice and was decreased by nintedanib treatments (Fig. 5E). The global biodistribution of [^{111}In]In-DOTAGA-AB0023 demonstrated that uptake was not different between NaCl-, BLM-receiving mice and BLM mice treated with nintedanib except in the lungs (Fig. 5F). Time curves of lung/blood and lung/muscle ratio confirm that nintedanib significantly reduced [^{111}In]In-DOTAGA-AB0023 lung uptake (Supplemental fig. 6D, E). Interestingly, immunostainings performed on a separate subset of animals demonstrated *ex vivo* than nintedanib was able to diminish the BLM-induced upregulation of LOXL2 expression in the lungs (Supplemental Fig. 7).

Most interestingly, the analysis of publicly available RNA sequencing datasets (GSE53845) demonstrated that LOXL2 gene expression was upregulated in IPF patients compared with healthy controls (Supplemental Fig. 8). These findings further highlight the potential of LOXL2 as a theranostic target in IPF.

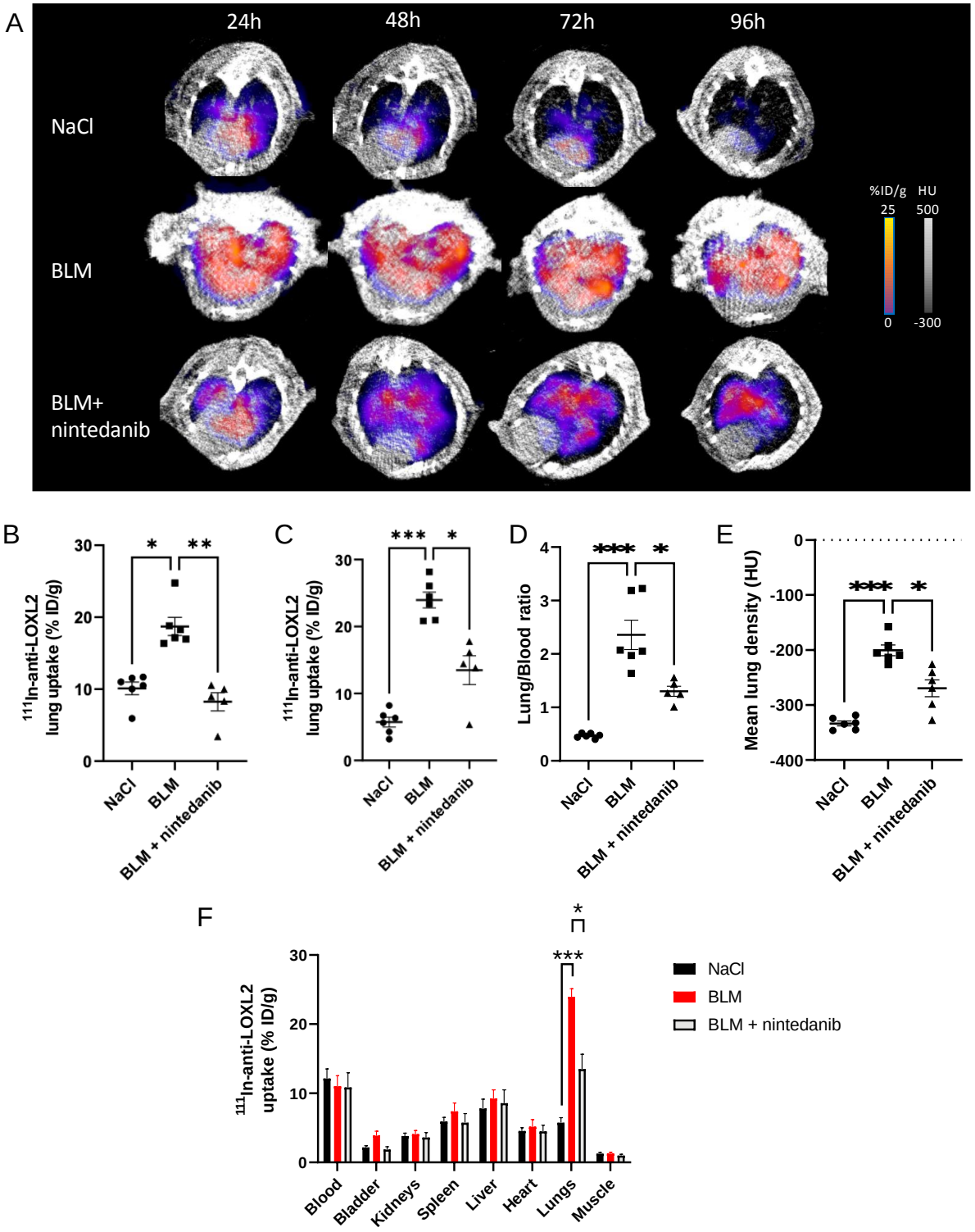

*Fig. 5: Nintedanib reduces lung fibrosis which can be detected by [^{111}In]In-DOTAGA-AB0023 SPECT imaging A/ Representative lung SPECT/CT images with [^{111}In]In-DOTAGA-AB0023 of NaCl-, BLM-receiving mice and BLM-receiving mice treated with nintedanib at D18 at 24h, 48h, 72h and 96h p.i.. B/ Graph represents the [^{111}In]In-DOTAGA-AB0023 lung uptake in %ID/g measured on SPECT images at 96h p.i. of NaCl- and BLM-receiving mice at D18. Results are presented as mean ± SEM, NaCl n=6, BLM n=6, BLM+nintedanib n=6. Difference between groups were compared using Kruskal-Wallis non-parametric ANOVA, *p<0.05, **p<0.01. C/ Graph represents the [^{111}In]In-DOTAGA-AB0023 lung uptake in %ID/g measured by gamma-counting 96h p.i. of NaCl-, BLM-receiving mice and BLM-receiving mice treated with nintedanib at D18. Results are presented as mean ± SEM. Difference between groups were compared using Kruskal-Wallis*

*non-parametric ANOVA, *p<0.05, ***p<0.001. D/ Graph represents the lung/blood ratio of [^{111}In]In-DOTAGA-AB0023 uptL2ke in %ID/g measured by gamma-counting 96h p.i. of NaCl-, BLM-receiving mice and BLM-receiving mice treated with nintedanib at D18. Results are presented as mean ± SEM, Difference between groups were compared using Kruskal-Wallis non-parametric ANOVA, *p<0.05, ***p<0.001. E/ Graph represents the mean lung density quantified on CT images of NaCl-, BLM-receiving mice and BLM-receiving mice treated with nintedanib at D18. Results are presented as mean ± SEM. Difference between groups were compared using Kruskal-Wallis non-parametric ANOVA, *p<0.05, ***p<0.001. F/ Graph represents the [^{111}In]In-DOTAGA-AB0023 uptake in %ID/g measured by gamma counting in blood, heart, kidney, bladder, liver, spleen,muscle and lungs of NaCl-, BLM-receiving mice and BLM-receiving mice treated with nintedanib at D18. Difference between groups were compared using Kruskal-Wallis non-parametric ANOVA, *p<0.05, ***p<0.001.*

Discussion

The identification of biomarkers of disease progression and therapy efficacy has become a hot topic in the lung fibrosis field in the last decade. The heterogeneous nature of IPF progression and the variability of response observed in patients under anti-fibrotic treatments is a major clinical concern leading to poorer outcome. While most of the attention has been focused on the discovery and evaluation of circulating biomarkers [31], *in vivo* molecular imaging recently emerged as a valuable tool to non-invasively assess the expression of various proteins involved in fibrosis progression [32]. In this context, our study aimed at developing an imaging probe targeting LOXL2. LOXL2 is a major protein involved in fibrogenesis as it is responsible for the cross-linking of the excessive amount of collagen in the fibrotic lung, thus leading to lung tissue stiffening and increased mechanical stretch which is a contributor of disease progression [33]. Our strategy was based on the bioconjugation of a murine anti-LOXL2 antibody, AB0023, with the chelator DOTAGA which has proven to be a valuable alternative to the standard DOTA [34]. To achieve reproducible results and control the degree of labeling, we opted for a site-specific enzymatic bioconjugation strategy using mTGase. This enzyme reacts on glutamine-295 residues, forming isopeptidic bonds with amine-functionalized probes [35]. PNGase F was first used to remove the glycan chains on asparagine-297 residues, leaving access to mTGase to react. Higher DOL than expected appeared during conjugation step, suggesting that there are two more reactive positions on this antibody. However, the conjugation of DOTAGA on AB0023 did not affect its affinity for LOXL2.

In clinic, the imaging of IPF is currently limited to high-resolution computed tomography (HRCT) both for diagnosis and monitoring, with little impact on mortality and therapeutic decision in IPF [36–38]. Indeed, lesions detected on HRCT may reflect a too advanced stage of the disease in patients for effective therapeutic intervention. In addition, while HRCT may inform on the extent of lung fibrosis at a given time, it does not account for activated molecular mechanisms that could be triggered for therapeutic purposes. Moreover, the recent approval of pirfenidone and nintedanib implies the implementation of strategies, which are not yet available, to monitor efficacy of these novel therapies in order to improve patient management and clinical outcome in IPF. Despite the fact that these two molecules have been shown to reduce lung function decline and to improve patients' survival in several clinical trials [39], their use is currently limited due to a high interpersonal variability among IPF patients. The lack of tools to accurately monitor pirfenidone and nintedanib efficacy in patients is another reason limiting their efficacy in the clinical practice. Considering the disabling side effects which may be associated to these therapies, the early prediction of treatment efficacy is a major clinical

issue. As a consequence, identifying novel imaging predictive biomarkers to predict/monitor therapeutic efficacy would be the first step towards a personalized management of IPF patients. Our results confirm previous reports demonstrating an increase in LOXL2 expression in the fibrotic lungs upon BLM stimulation [11]. As expected for a full length antibody, which has slow distribution times, the optimal imaging time of [^{111}In]In-DOTAGA-AB0023 was between 72 h and 96 h post-injection. Our results are comparable to recent studies highlighting the interest of molecular imaging to follow other biomarkers. John *et al*. developed a specific peptide to the integrin $\alpha_V\beta_6$ (A20FMDV2) radiolabeled with ^{111}In to measure $\alpha_V\beta_6$ expression in BLM-treated mouse lungs by SPECT/CT [40]. Overexpression of $\alpha_V\beta_6$ integrin by alveolar epithelial cells plays a crucial role in the pathogenesis of pulmonary fibrosis by favoring TGF-β1 activation. Lung uptake of ^{111}In-A20FMDV2 was increased in BLM-treated mice compared to control mice. Quantitative analysis demonstrated that SPECT signals correlate with the levels of collagen, $\alpha_V\beta_6$ protein, and messenger RNA of the β_6 subunit [40]. Very recently the lung uptake of the same peptide modified with fluorine-18 for PET imaging ([^{18}F]FB-A20FMDV2) has been shown to be increased in a small cohort of patients with IPF compared with healthy controls [41]. Following the same concept, Désogère *et al*. developed a peptide-based PET probe ([^{68}Ga]Ga-CBP8) which targets collagen type I for lung fibrosis imaging [42]. The authors demonstrate high specificity of [^{68}Ga]Ga-CBP8 for pulmonary fibrosis *in vivo* in bleomycin-treated mice. In addition, [^{68}Ga]Ga-CBP8 signals correlated with lung collagen content and showed sensitivity to monitor response to treatment in bleomycin-induced lung fibrosis [42]. Similarly, imaging of Fibroblast Activation Protein-α (FAP), a membrane marker of fibroblasts activation, with radiolabeled quinoline-based small molecule (FAPI) has been shown to noninvasively detect disease activity in a murine model of pulmonary fibrosis [43] Interestingly, PET imaging with [^{68}Ga]Ga-radiolabeled FAPI has the potential to detect the early onset of fibrotic injury to promote early diagnosis. A recent clinical study confirms these findings by demonstrating an increase in [^{68}Ga]Ga-FAPI lung uptake in IPF patients compared with healthy volunteers [44]. Contrary to our study, most of the developed tracers for lung fibrosis imaging rely on small peptides instead of full length antibodies. While small peptides present the advantage to display a short biodistribution profile favorable for imaging purposes, they also present much lower accumulation rates in targeted organs which may worsen the interpretation of images due to a weak signal-to-background ratio. In our study, the lung accumulation of [^{111}In]In-DOTAGA-AB0023 in fibrotic lungs is approximately three to four fold higher than in non-fibrotic lungs. In addition, accumulation of [^{111}In]In-DOTAGA-AB0023 is approximately three-fold higher in the lungs compared with blood and muscles which are not expressing LOXL2. These results demonstrate a high signal-to-background ratio allowing an accurate evaluation of [^{111}In]In-DOTAGA-AB0023 lung accumulation in the context of fibrosis. Nevertheless, the evaluation of imaging properties of smaller fragments of AB0023 (*e.g.* Fab or F(ab')$_2$) may be of interest in future studies. Despite promising preclinical results, the inhibition of LOXL2 with simtuzumab, the humanized monoclonal antibody corresponding to AB0023, failed in a large phase 2 study (RAINIER trial) that examined the efficacy of simtuzumab for the treatment of IPF. Benefit of simtuzumab over placebo was not shown for the endpoints of progression-free survival, all-cause hospitalizations, and mortality as well as decline in FVC % predicted, diffusing capacity of the lung (DLCO) % predicted, and 6-min walk distance. This trial enrolled a large number of patients (544) which were stratified based on LOXL2 serum levels to increase chances of success. Nevertheless, whether the level of circulating LOXL2 is correlated with its lung expression remains to be fully elucidated. In this context, imaging tools such as [^{111}In]In-DOTAGA-AB0023 may be of great value to

stratify patients based on LOXL2 lung expression levels to select patients more likely to respond to anti-LOXL2 therapies. This strategy may represent a first step towards precision medicine for the treatment of patients with IPF. It has been suggested that the failure of the RAINIER trial was due to poor tissue penetration in the human IPF lung thus leading to a non-optimal LOXL2 inhibition [45]. Our results demonstrate that [^{111}In]In-DOTAGA-AB0023 was able to reach and specifically remain in the lungs in fibrotic areas where LOXL2 is most likely overexpressed. Such tools may be of interest to assess tissue penetration of full-length antibodies such as simtuzumab in human IPF lungs. Additionally, LOXL2 is only one of the family of LOXL enzymes that are involved in collagen crosslinking, and the non-LOXL2 enzymes were not susceptible to selective allosteric inhibition by simtuzumab. For instance, LOXL1 has been demonstrated to also play a crucial role in lung fibrosis [46] suggesting that therapeutic strategies involving co-inhibition of LOXL2 with other crosslinking enzymes such as LOXL1 may be of interest.

Finally, our study reveals that in our preclinical model nintedanib seems to decrease lung LOXL2 expression. Clinicians are currently unable to identify responders versus non-responders before starting antifibrotic treatments nintedanib and pirfenidone, and do not know whether declining lung function during treatment indicates a lack of response to one of the drugs or whether lung function decline has been significantly attenuated and would have declined more rapidly without antifibrotic treatment. In this context, the use of an imaging agent such as [^{111}In]In-DOTAGA-AB0023 may represent a non-invasive strategy to longitudinally monitor efficacy of antifibrotic treatments.

Conclusion

The use of an enzymatic site-specific conjugation strategy has led to the reliable and reproducible production of the first anti-LOXL2 SPECT tracer. The radioimmunoconjugate showed promising results in a preclinical model of bleomycin-induced lung fibrosis, with a high lung uptake. The ability of AB0023 to monitor the response to nintedanib was also investigated and demonstrate encouraging outcomes. Our study offers a first proof of concept of the use of a non-invasive and accurate strategy to monitor LOXL2 expression that may help, in the future, patients' stratification for potential clinical trials assessing anti-LOXL2 strategies in IPF, a first step toward personalized management of IPF patients.

Acknowledgments

This work was supported by France Life Imaging (ANR-11-INBS-0006 grant from the French "Investissements d'Avenir" program, Project ImaFibro), the Centre National de la Recherche Scientifique (CNRS), the Université de Bourgogne, the Conseil Régional de Bourgogne Franche-Comté, the European Union through the PO FEDER-FSE 2014/2020 Bourgogne program. This project was supported by « Agence National de la Recherche » (HYMAGE-IPF: ANR-20-CE17-0005).

The authors thank the Plateforme d'Analyse Chimique et de Synthèse Moléculaire de l'Université de Bourgogne (http://www.wpcm.fr) for access to analytical instrumentation.

Supporting information file

HPLC-MS analysis of reduced DOTAGA-AB0023, HPLC-MS/MS analysis of DOTAGA-AB0023 after tryptic digestion, Radio-iTLC chromatogram and *in vitro* stability in plasma of [^{111}In]In-DOTAGA-AB0023 , Individual SPECT and CT images, Time-curves for lung/blood and lung/muscle ratios, IHC of LOXL2, LOXL2 mRNA expression in healthy controls and IPF patients.

References

1. Tanzer ML. Cross-linking of collagen. Science. 1973;180:561–6.
2. Maher TM, Bendstrup E, Dron L, Langley J, Smith G, Khalid JM, et al. Global incidence and prevalence of idiopathic pulmonary fibrosis. Resp Res. 2021;22:197.
3. Martinez FJ, Collard HR, Pardo A, Raghu G, Richeldi L, Selman M, et al. Idiopathic pulmonary fibrosis. Nat Rev Dis Primers. 2017;3:1–19.
4. Kaarteenaho R. The current position of surgical lung biopsy in the diagnosis of idiopathic pulmonary fibrosis. Respir Res. 2013;14:43.
5. Lamas DJ, Kawut SM, Bagiella E, Philip N, Arcasoy SM, Lederer DJ. Delayed access and survival in idiopathic pulmonary fibrosis: a cohort study. Am J Respir Crit Care Med. 2011;184:842–7.
6. Moon H-J, Finney J, Ronnebaum T, Mure M. Human Lysyl Oxidase-like 2. Bioorg Chem. 2014;57:231–41.
7. Chien JW, Richards TJ, Gibson KF, Zhang Y, Lindell KO, Shao L, et al. Serum lysyl oxidase-like 2 levels and idiopathic pulmonary fibrosis disease progression. Eur Respir J. 2014;43:1430–8.
8. Almassian B, Trackman PC, Iguchi H, Boak A, Calvaresi D, Kagan HM. Induction of lung lysyl oxidase activity and lysyl oxidase protein by exposure of rats to cadmium chloride: properties of the induced enzyme. Connect Tissue Res. 1991;25:197–208.
9. Matsuo A, Tanida R, Yanagi S, Tsubouchi H, Miura A, Shigekusa T, et al. Significance of nuclear LOXL2 inhibition in fibroblasts and myofibroblasts in the fibrotic process of acute respiratory distress syndrome. Eur J Pharmacol. 2021;892:173754.
10. Aumiller V, Strobel B, Romeike M, Schuler M, Stierstorfer BE, Kreuz S. Comparative analysis of lysyl oxidase (like) family members in pulmonary fibrosis. Sci Rep. 2017;7:149.
11. Barry-Hamilton V, Spangler R, Marshall D, McCauley S, Rodriguez HM, Oyasu M, et al. Allosteric inhibition of lysyl oxidase-like-2 impedes the development of a pathologic microenvironment. Nat Med. 2010;16:1009–17.
12. Wen X, Liu Y, Bai Y, Li M, Fu Q, Zheng Y. LOXL2, a copper-dependent monoamine oxidase, activates lung fibroblasts through the TGF-β/Smad pathway. Int J Mol Med. 2018;42:3530–41.
13. Mehal WZ, Iredale J, Friedman SL. Scraping fibrosis: expressway to the core of fibrosis. Nat Med. 2011;17:552–3.
14. Friedman SL, Sheppard D, Duffield JS, Violette S. Therapy for fibrotic diseases: nearing the starting line. Sci Transl Med. 2013;5:167sr1.
15. Ahluwalia N, Shea BS, Tager AM. New Therapeutic Targets in Idiopathic Pulmonary Fibrosis. Aiming to Rein in Runaway Wound-Healing Responses. Am J Respir Crit Care Med. 2014;190:867–78.
16. Verstovsek S, Savona MR, Mesa RA, Dong H, Maltzman JD, Sharma S, et al. A phase 2 study of simtuzumab in patients with primary, post-polycythaemia vera or post-essential thrombocythaemia myelofibrosis. Br J Haematol. 2017;176:939–49.
17. Puente A, Fortea JI, Cabezas J, Arias Loste MT, Iruzubieta P, Llerena S, et al. LOXL2—A New Target in Antifibrogenic Therapy? Int J Mol Sci. 2019;20:1634.
18. Harrison SA, Abdelmalek MF, Caldwell S, Shiffman ML, Diehl AM, Ghalib R, et al. Simtuzumab Is Ineffective for Patients With Bridging Fibrosis or Compensated Cirrhosis Caused by Nonalcoholic

Steatohepatitis. Gastroenterology. 2018;155:1140–53.
19. Muir AJ, Levy C, Janssen HLA, Montano-Loza AJ, Shiffman ML, Caldwell S, et al. Simtuzumab for Primary Sclerosing Cholangitis: Phase 2 Study Results With Insights on the Natural History of the Disease. Hepatology. 2019;69:684–98.
20. Fickert P. Is This the Last Requiem for Simtuzumab? Hepatology. John Wiley & Sons, Ltd; 2019;69:476–9.
21. Raghu G, Brown KK, Collard HR, Cottin V, Gibson KF, Kaner RJ, et al. Efficacy of simtuzumab versus placebo in patients with idiopathic pulmonary fibrosis: a randomised, double-blind, controlled, phase 2 trial. The Lancet Resp Med. 2017;5:22–32.
22. Wuest M, Kuchar M, Sharma SK, Richter S, Hamann I, Wang M, et al. Targeting lysyl oxidase for molecular imaging in breast cancer. Breast Cancer Res. 2015;17:107.
23. Hutchinson JH, Rowbottom MW, Lonergan D, Darlington J, Prodanovich P, King CD, et al. Small Molecule Lysyl Oxidase-like 2 (LOXL2) Inhibitors: The Identification of an Inhibitor Selective for LOXL2 over LOX. ACS Med Chem Lett. 2017;8:423–7.
24. Ferreira S, Saraiva N, Rijo P, Fernandes AS. LOXL2 Inhibitors and Breast Cancer Progression. Antioxidants (Basel). 2021;10:312.
25. Findlay AD, Foot JS, Buson A, Deodhar M, Jarnicki AG, Hansbro PM, et al. Identification and Optimization of Mechanism-Based Fluoroallylamine Inhibitors of Lysyl Oxidase-like 2/3. J Med Chem. 2019;62:9874–89.
26. Verstovsek S, Mascarenhas J, Rampal RK, Cilloni D, Harrison C, Jacoby B, et al. Mylox-1: An Open-Label, Phase IIa Study of the Safety, Tolerability, Pharmacokinetics and Pharmacodynamics of Oral LOXL2 Inhibitor, GB2064, in Myelofibrosis. Blood. 2022;140:3868–70.
27. Jenkins RG, Moore BB, Chambers RC, Eickelberg O, Königshoff M, Kolb M, et al. An Official American Thoracic Society Workshop Report: Use of Animal Models for the Preclinical Assessment of Potential Therapies for Pulmonary Fibrosis. Am J Respir Cell Mol Biol. 2017;56:667–79.
28. Kolb P, Upagupta C, Vierhout M, Ayaub E, Bellaye PS, Gauldie J, et al. The importance of interventional timing in the bleomycin model of pulmonary fibrosis. Eur Respir J. 2020;55:1901105.
29. Tanguy J, Goirand F, Bouchard A, Frenay J, Moreau M, Mothes C, et al. [18F]FMISO PET/CT imaging of hypoxia as a non-invasive biomarker of disease progression and therapy efficacy in a preclinical model of pulmonary fibrosis: comparison with the [18F]FDG PET/CT approach. Eur J Nucl Med Mol Imaging. 2021;48:3058–74.
30. Liu H, Gaza-Bulseco G, Faldu D, Chumsae C, Sun J. Heterogeneity of Monoclonal Antibodies. J Pharm Sci. 2008;97:2426–47.
31. Adegunsoye A, Alqalyoobi S, Linderholm A, Bowman WS, Lee CT, Pugashetti JV, et al. Circulating Plasma Biomarkers of Survival in Antifibrotic-Treated Patients With Idiopathic Pulmonary Fibrosis. Chest. 2020;158:1526–34.
32. Broens B, Duitman J-W, Zwezerijnen GJC, Nossent EJ, van der Laken CJ, Voskuyl AE. Novel tracers for molecular imaging of interstitial lung disease: A state of the art review. Autoimmun Rev. 2022;21:103202.
33. Froese AR, Shimbori C, Bellaye P-S, Inman M, Obex S, Fatima S, et al. Stretch-induced Activation of Transforming Growth Factor-β1 in Pulmonary Fibrosis. Am J Respir Crit Care Med. 2016;194:84–96.
34. Bernhard C, Moreau M, Lhenry D, Goze C, Boschetti F, Rousselin Y, et al. DOTAGA–Anhydride: A Valuable Building Block for the Preparation of DOTA-Like Chelating Agents. Chem Eur J. 2012;18:7834–41.

35. Jeger S, Zimmermann K, Blanc A, Grünberg J, Honer M, Hunziker P, et al. Site-Specific and Stoichiometric Modification of Antibodies by Bacterial Transglutaminase. Angew Chem Int Ed. 2010;49:9995–7.
36. Raghu G, Collard HR, Egan JJ, Martinez FJ, Behr J, Brown KK, et al. An official ATS/ERS/JRS/ALAT statement: idiopathic pulmonary fibrosis: evidence-based guidelines for diagnosis and management. Am J Respir Crit Care Med. 2011;183:788–824.
37. Noth I, Martinez FJ. Recent advances in idiopathic pulmonary fibrosis. Chest. 2007;132:637–50.
38. Raghu G, Weycker D, Edelsberg J, Bradford WZ, Oster G. Incidence and prevalence of idiopathic pulmonary fibrosis. Am J Respir Crit Care Med. 2006;174:810–6.
39. Fujimoto H, Kobayashi T, Azuma A. Idiopathic Pulmonary Fibrosis: Treatment and Prognosis. Clin Med Insights Circ Respir Pulm Med. 2015;9:179–85.
40. John AE, Luckett JC, Tatler AL, Awais RO, Desai A, Habgood A, et al. Preclinical SPECT/CT imaging of αvβ6 integrins for molecular stratification of idiopathic pulmonary fibrosis. J Nucl Med. 2013;54:2146–52.
41. Lukey PT, Coello C, Gunn R, Parker C, Wilson FJ, Saleem A, et al. Clinical quantification of the integrin αvβ6 by [18F]FB-A20FMDV2 positron emission tomography in healthy and fibrotic human lung (PETAL Study). Eur J Nucl Med Mol Imaging. 2020;47:967–79.
42. Désogère P, Tapias LF, Hariri LP, Rotile NJ, Rietz TA, Probst CK, et al. Type I collagen-targeted PET probe for pulmonary fibrosis detection and staging in preclinical models. Sci Transl Med. 2017;9:eaaf4696.
43. Rosenkrans ZT, Massey CF, Bernau K, Ferreira CA, Jeffery JJ, Schulte JJ, et al. [68 Ga]Ga-FAPI-46 PET for non-invasive detection of pulmonary fibrosis disease activity. Eur J Nucl Med Mol Imaging [Internet]. 2022 [cited 2022 May 24]; Available from: https://doi.org/10.1007/s00259-022-05814-9
44. Yang P, Luo Q, Wang X, Fang Q, Fu Z, Li J, et al. Comprehensive Analysis of Fibroblast Activation Protein Expression in Interstitial Lung Diseases. Am J Respir Crit Care Med. 2023;207:160–72.
45. Meyer KC. Great expectations for simtuzumab in IPF fall short. Lancet Respir Med. 2017;5:2–3.
46. Bellaye P-S, Shimbori C, Upagupta C, Sato S, Shi W, Gauldie J, et al. Lysyl Oxidase–Like 1 Protein Deficiency Protects Mice from Adenoviral Transforming Growth Factor-β1–induced Pulmonary Fibrosis. Am J Respir Cell Mol Biol. 2018;58:461–70.